IEEE Access
Multidisciplinary | Rapid Review | Open Access Journal

Received 7 July 2022, accepted 5 September 2022, date of publication 8 September 2022, date of current version 19 September 2022.

Digital Object Identifier 10.1109/ACCESS.2022.3205408

APPLIED RESEARCH

Space Qualification of Metalized Additive Manufactured Filters

CARMEN BACHILLER, VICENTE NOVA, ÁLVARO FERRER, AND VICENTE E. BORIA ESBERT, (Fellow, IEEE)
Instituto de Telecomunicaciones y Aplicaciones Multimedia, Universitat Politècnica de València, 46022 Valencia, Spain

Corresponding author: Carmen Bachiller (mabacmar@dcom.upv.es)

This work was supported in part by the Agencia Valenciana de la Innovación Research Project under Grant INNVA1/2020/84; in part by the Agencia Estatal de Investigación, Spain, through the Fellowship for Training PhDs under Grant BES-2017-079728; and in part by the Ministerio de Ciencia e Innovación (MICIN), Spanish Government through the Research and Development Project PID2019-103982RB-C41 under Grant MICIN/AEI/10.13039/501100011033.

ABSTRACT The space industry is seeking new solutions for the development of lightweight, inexpensive and easy-to-manufacture on-board communication payload devices. One of the proposed technologies is additive manufacturing (AM) of polymeric materials that are subsequently metallized. The devices developed using this technique must be operational in the particular space environment conditions. In this work we study the integrity of filters made by additive manufacturing against the extreme conditions of mechanical stress, temperature and power management as described in the standard of the European Space Agency (ESA) for satellite payload. To carry out this qualification for space, two types of X-band filters with identical frequency responses have been designed and manufactured: a classic H-plane waveguide cavities filter, and three filters on surface-mount technology (SMT). Two of the SMT filters are low height rectangular cavities filters, while the third one is a high circular cavities filter. This selection was intended to verify that the AM technique offered good results regardless of the devices topology. Two mechanical vibration tests were performed: sinusoidal sweep and random vibration. These tests emulate the transport and launching conditions of the satellite payload. Furthermore, it was measured the mechanical natural frequency of the filters, and its variation after being exposed to the tests in order to evaluate their physical integrity. The thermal analysis was performed emulating the temperature profile experienced by the satellite payload during working conditions. Then, the power handling tests were carried out. The secondary electron emission yield of the material (metallized polymer) was firstly measured. The power levels, location and frequency at which a multipactor discharge would occur were analyzed for both, low-height and standard-height, filters. Finally, both filters were subjected to those power levels, under high vacuum conditions, to check if the said multipactor discharges occurred. The mechanical stress and temperature tests prove that the developed filters can survive the hard launching and operation conditions of commercial satellite payloads. The multipactor tests report the high power levels that the devices can handle without risk of radiofrequency (RF) breakage. All these tests allow to fully qualify the proposed manufacturing technique for spatial applications.

INDEX TERMS Filters, space qualification, multipactor, natural frequency, space communications, temperature, vibration, additive manufacturing.

I. INTRODUCTION

Current communication systems face increasingly complex challenges. On the one hand, new services and applications entail a growing need for bandwidth, which leads to the search for even higher frequency bands and a more efficient use of them. In addition, the ubiquitous internet access advocated by the Internet of Things (IoT) [1], [2] is translating into an exponential increase in launches of small low-earth orbit (LEO) satellites [3], [4], as an example from 20 satellites

The associate editor coordinating the review of this manuscript and approving it for publication was Aniruddha Datta.

launched in 2011 to more than 350 in 2021. These new small-size satellites require the development of passive components and antennas of low weight and volume, with lower manufacturing costs and high performance. On the other hand, the industry has been searching for new manufacturing technologies for communications devices that provide an alternative to the classical fabrication methods of metal waveguides. The challenge is to achieve light, low-cost (both for prototyping and manufacturing) devices, with features similar to standard waveguide devices, whilst optimizing the use of expensive conductive metals. Furthermore, they should be integrated with the rest of the systems, usually on planar technology.

One of the current trends is the use of additive manufacturing for the development of passive communication devices, such as resonators [5], filters [6] and antennas [7]. This technology allows the manufacture of a wide range of topologies, many of which cannot be achieved with the traditional use of moulding or milling on metal. AM allows both to implement classic topologies, such as rectangular waveguide cavity filters, and to explore newer ones, such as surface mounted devices that can be integrated with planar circuit boards (PCBs) thanks to ad-hoc developed transitions. In addition, the devices can be manufactured using polymers that are subsequently metallized, with the consequent reduction in weight and cost. Since this is a novel technology, new materials and processes appear every day. The scientific community has put a lot of effort into developing 3D printed communication devices. However, much work remains to be done if they are going to be used in space communications.

The different space agencies define the set of test that the satellite and its payload must pass before launching it. The on-board communications devices must prove their viability in front of extreme conditions of mechanical vibration, temperature change and power handling, among others. This process is commonly known as ''qualification for space applications''. Examples of this process can be found in [8], where a complete space qualification is performed on a traditional waveguide filter. In [6] temperature tests are performed on 3D printed waveguide filters. Additionally, regarding substrate-integrated circuits (SICs), [9] performs temperature and power handling testing, but not mechanical tests, on Air-Filled SIW (AFSIW) filters and multiplexers. Later on, [10] performs a thermal analysis under atmospheric pressure and high vacuum conditions on a set of SIC filters of different topologies and embodiments, whilst [11] carries our vibration tests on these same filters.

Since AM is an experimental technology for the development of many communication devices, its performance must be assessed from different points of view. Few tests have been made in order to validate these technologies for space applications, where the devices have to stand extreme temperature variations, strong mechanical stress and high-vacuum conditions.

This work aims to assess the feasibility of AM X-band communications filters to operate under space conditions. Two types of filters were developed: the first type is based on standrad WR-75 waveguides, and the second one using the surface-mount technology (SMT). Three types of tests were conducted: mechanical vibration tests, thermal analysis and power handling tests, as described in the European Space Agency standard ECSS-E-ST-10-03C [12]. Section III presents mechanical vibration tests, which emulate the stress levels under the vibratory stress conditions that these devices suffer during satellite transport and launching stages. Section IV shows the thermal analysis made to emulate the temperature shift that a LEO satellite payload suffer during operation. Finally, Section V deals with power handling tests, including secondary emission yield characterization, outgassing and multipactor discharge, thus obtaining the power level the device can handle without risk of RF breakdown.

II. METALIZED ADDITIVE MANUFACTURING FILTERS

Three different implementations of band-pass filter have been considered: a WR75 classical filter, an SMT filter of low profile and rectangular cavities (R-SMT), and an SMT filter of high height and circular cavities (C-SMT). The classical WR75 filter is intended to be used in demanding applications such as big geostationary (GEO) satellites, where high power, high isolation and low loss are needed. In contrast, SMT filters are focused on small satellite applications, where low cost, low volume, and easy interconnection and assembling with planar systems are crucial.

The proposed filters were designed to implement a four-poles Chebyshev band-pass filter centred at 11 GHz, with 300 MHz of bandwidth and 20 dB of maximum return loss (RL) level (0.05 dB of ripple) in the passband.

Filters' topology is shown in Figure 1. They consist of circular or rectangular cavity resonators internally coupled by shunt inductance irises. The classical WR75 filter is fed by a standard UDR 120 flange, whereas SMT filters are externally coupled to a microstrip line through a slot transition [13]. In the last configuration, the slot transition works as the input/output coupling of the filters, thus reducing the total length of the device, and simplifying the design process by eliminating the necessity of broadband transitions.

Filters were designed by following the coupling matrix synthesis method described in [14], in which coupling elements and resonators are synthesised into the filters' physical dimensions by using a numerical electromagnetic simulator (CST Studio Suite v.2021, CST GmbH, now with Dassault Systèmes). The WR75 filter is based on a standard WR75 waveguide with a width of 19.05 mm and a height of 9.525 mm. Filter's resonators (TE_{101} mode) are about 16 mm length, and as can be seen in Figure 1 (a), some holes have been performed on this device to fit the multipactor venting requirements. The C-SMT filter is based on cylindrical resonators (TM_{010} mode) with a diameter of about 20 mm and a height of 10 mm, see Figure 1 (b). The R-SMT filter, Figure1 (c), is based on a rectangular resonator (TE_{101} mode) with 19.05 mm of width, 2 mm of height, and about

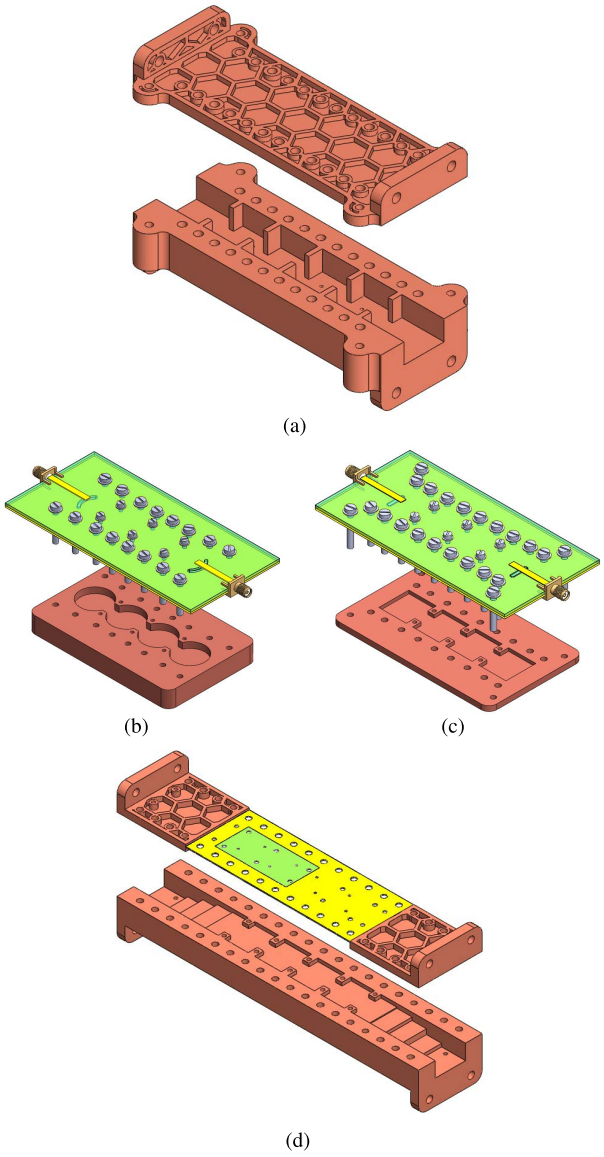

FIGURE 1. 3D view of the proposed filter: (a) is the WR75 filter, (b) is the SMT filter based on circular cavities (C-SMT), (c) is the SMT filter based on rectangular cavities (R-SMT), and (d) is the equivalent model of the SMT filter based on rectangular cavities with a transition to rectangular waveguide (low profile filter). Green is the PCB substrate, yellow is the PCB copper, and light red is the metallised additive manufactured part.

17 mm of length. Both SMT filters are fed by a microstrip line integrated into a RO4003C PCB with a height of 1.524 mm.

Proposed filters are subjected to three different space qualification tests: vibration shock (section III), thermal cycling (section IV), and multipactor (section V). These tests impose some constraints and modifications on the geometry of the devices that are explained in the different testing sections of this paper. However, it is important to mention that the expected multipactor breakdown power of SMT filters was higher than the maximum power supported by usual coaxial connectors. This implies that SMT filters cannot be subjected to multipactor tests with the slot transition, so it was redesigned to be fed by a standard UDR 120 flange while maintaining a PCB cover, see Figure 1 (d). Since the height and materials of both implementations are the same, both realisations are identical from a multipactor point of view. Moreover, the proposed feeding allows employing the same multipactor test bench for the WR75 filter and the low profile realisations.

Filters were SLA-printed with a commercial glass-filled photosensitive resin, Rigid-10k from Formlabs [15], with a printing resolution of 25 μm. The use of glass-filled resin improves printing accuracy, and increases the heat deflection temperature (HDT) and tensile strength compared to traditional resins. This is especially appropriate for space applications where there are high-temperature gradients and mechanical shocks.

Filters were printed in such a way that they do not need supports neither inside the filters' cavities nor in the contact areas with PCBs and covers. Once the device is printed, it is firstly plated by using an electroless plating process (also known as autocatalytic plating), which is used as seed layer to apply a final electroplating. This two step metallisation process has finally achieved an homogeneous copper layer from 6.5 to 12 μm.

On the other hand, the PCB of SMT integrated filters was manufactured on RO4003C substrate of 1.5 mm of thickness with a double cladding of 17 μm of copper using a Protomat 103S milling machine from LPKF. It is important to note that the proposed slot transition does not need any plating process, which drastically reduces the manufacturing complexity and cost of the PCB.

Figures 2. (a), (b), (c) and (d) show the frequency responses of the proposed filters. Measurements agree well with simulations. Deviations are mainly due to manufacturing tolerances and assembling gaps, being the C-SMT filter the most robust against these undesired effects.

III. VIBRATION TESTS

The objective of mechanical vibration tests is to ensure the structural and functional integrity of the devices when they are subjected to strong mechanical waves. Mechanical stress wave-based disturbances can cause deformations in the materials through which they propagate. These deformations can lead to irreversible structural changes depending on the stress frequency, duration, amplitude and the mechanical characteristics of the materials. These stress phenomena are characteristic of any space application due to the intense vibrations during take-off and orbit positioning. For these applications, the technical characteristics of these tests, as well as the associated tolerance margins, are specified by the space agencies. In particular, in this work we used the ECSS-E-ST-10-03C standard [12] of the European Space Agency (ESA). Three different tests are defined for this purpose in the ECSS standard: sweep test, random vibration, and shock wave test.

Additionally, the concept of natural frequency is of particular interest. This is the resonance frequency at which a system tends to oscillate without external forces. The variation of the frequency and amplitude in this oscillation is used in the

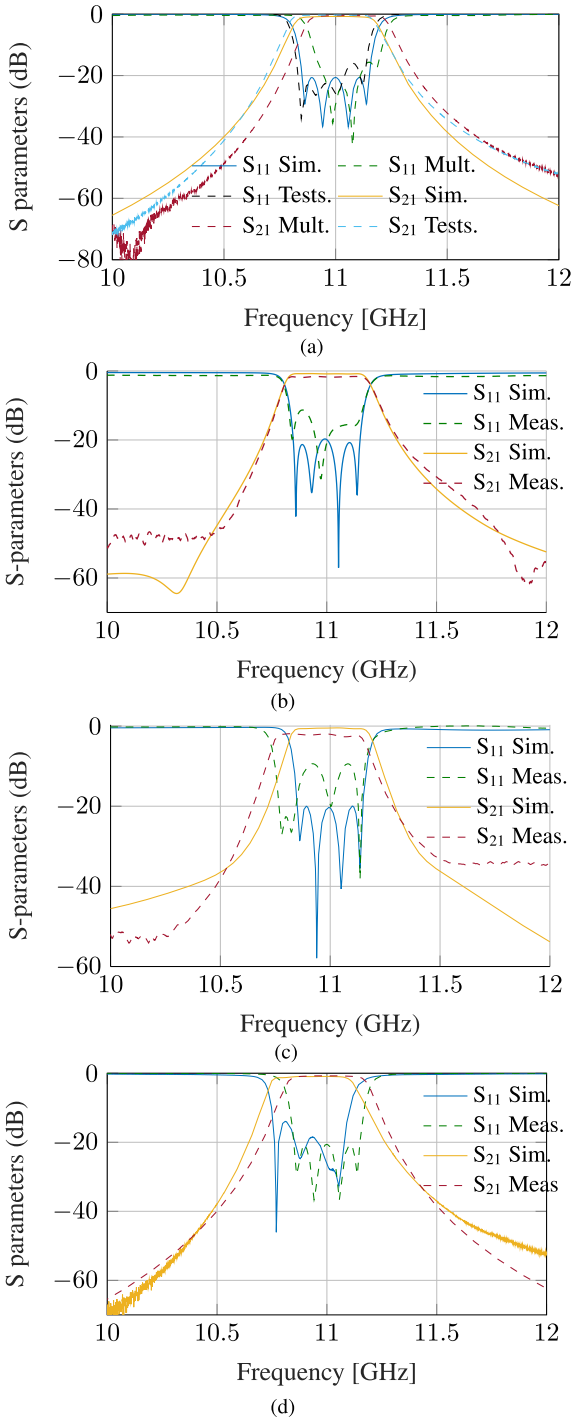

FIGURE 2. **Frequency responses (simulated and measured under room temperature conditions) of the proposed filters: (a) WR75 filter realisations (Mult. stands for multipactor test and Tests. stands for temperature and vibration tests), (b) C-SMT filter, (c) R-SMT filter, and (d) Rectangular low profile filter.**

standard to assess whether a device has successfully passed the vibration tests.

A. GENERAL CONSIDERATIONS

In this work sweep test, random vibration and measurement of the natural frequency were carried out on WR75 filter, SMT circular cavities filter (C-SMT) and SMT rectangular cavities filter (R-SMT).

The following actions must be observed while carrying out the vibration tests:

1) The tests have to be carried out in launch configuration for the three spatial axes (X, Y and Z).
2) The natural frequency of each device must be measured before and after the test, variation must be less than 5% in frequency and 20% in amplitude in order to pass the test.
3) Visual check must be carried out to verify the integrity of the devices.
4) The setup must not present resonances within the frequency band of the test.

Therefore, a specific setup and a set of tools capable of carrying out both tests and measurements were necessary. The vibrational response of the filters is influenced by the type of setup used in the tests. In this case, C-SMT and R-SMT filters were screwed to a 25 mm thick aluminium plate by using four M3 screws at the ends (see Figure 3), in the same way as they are fixed in the satellite payload panel. A specific support was built to screw the WR75 filter to the plate. As shown in Figure 3, the aluminium jig can be placed in different orientations, which enables the testing set for the three spatial axes.

The following tools were used for the excitation and measurements:

- Electrodynamics vibration exciter LDS V721: together with a PA1000 amplifier constitutes the vibrating bed that transmits the stress waves to the filters.
- Triaxial accelerometer PCB 356A16 (100 mV/g): it will be placed on the vibrating bed or on the aluminium support, depending on the test.
- Ultralight accelerometers PCB 352C22 (10 mV/g): precision accelerometers will be placed on the vibrating bed or on the filters themselves, depending on the measurement.
- National Instruments PCI 4451 card for the excitator management and measurement in the random vibration test.
- P8020 Analizer and Prosig DATS 7.0 software for the measurement of the natural frequencies.

To measure the natural frequencies, the above mentioned ultralight accelerometers were placed on the centre of each filter.

B. SINUSOIDAL SWEEP

Sinusoidal sweep consisted of applying narrow-band stress waves to the filters. During the test, the device is subjected to an incremental and decremental frequency sine vibration. According to the standard, it tries to assess the behaviour of the devices under low-frequency stress waves during the launching or ground transport processes.

For this test, we defined a profile of spectral density based on the values extracted from the Ariane 5 and 6, the Soyuz and

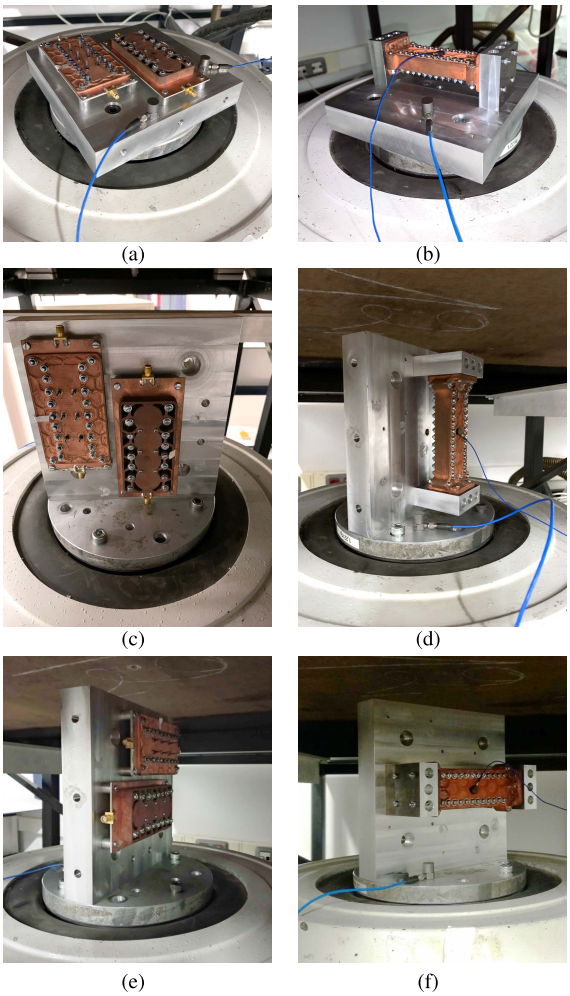

FIGURE 3. Setup for vibration tests: (a) SMT filters on Y-axis measurement configuration, (b) WR75 filter on Y-axis measurement configuration, (c) SMT filters on Z-axis measurement configuration, (d) WR75 filter on Z-axis measurement configuration, (e) SMT filters on X-axis measurement configuration, (f) WR75 filter on X-axis measurement configuration.

the Vega shuttles [16], [17] (in blue in Figure 4). In each of the three directions, a sweep has been made from 4 Hz to 140 Hz with an amplitude of 1.25 g and a sweep speed of 2 octaves per minute. To preserve the integrity of the electrodynamic exciter, between 4 Hz and 8.8 Hz, the maximum displacement amplitude has been limited to 4 mm, which implies that at 4 Hz the applied acceleration has been 0.26 g, reaching the acceleration of 1.25 g when the signal frequency reached 8.8 Hz. During the sweep, around 11 Hz the acceleration reached 1.4 g. Figure 4 shows in red the incremental and decremental applied excitation for the three directions.

C. RANDOM VIBRATION

This test evaluates the structural feasibility of the filters under broadband mechanical disturbances caused during the launching or ground transport processes. During the test, the device is subjected to a pseudo-random vibration signal, whose energy level is defined by an Amplitude Spectral

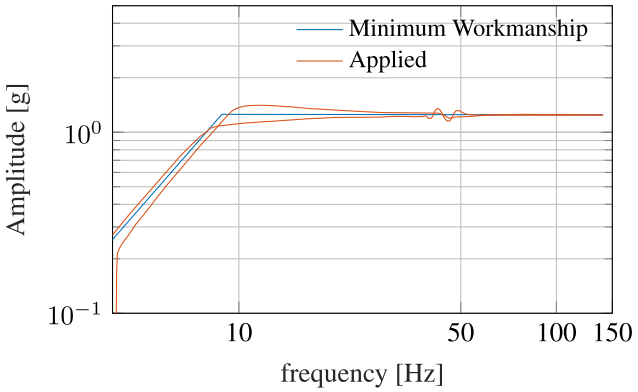

FIGURE 4. Amplitude Spectral Density (ASD) of vibration applied to filters in sinusoidal sweep.

Density (ASD). The signal can be described as non-correlated, and it is composed of multiple sinusoidal vibrations occurring simultaneously at different frequencies over a specific frequency range.

The spectral density of acceleration of the mechanical excitation induced in the devices must avoid peaks and not present slopes greater than 25 dB/octave. In addition, the standardxata [12] states that it must be 3 dB above the levels established in the minimum workmanship (MW). For defining the ASD profile of this test, the minimum workmanship of NASA, Ariane and Soyuz shuttles has been studied. Finally, only the minimum workmanships of the NASA and Soyuz shuttle were considered since the Ariane launcher replaced this test with an acoustic vibration test, for which we would need a completely different test bench. The resulting profile that fit both, the Soyuz shuttle and the NASA minimum workmanship, is depicted in blue in Figures 5 and 6.

A broadband vibration with frequency content between 20 Hz and 2 kHz has been applied in each of the three test directions for the three filters. The duration of the vibration applied in each direction was 2 minutes and the theoretical root mean square (RMS) of the vibration in that band was 8.02 g, reaching peaks of 40 g.

The acceleration of the vibrating table during the test has been recorded, showing in Figure 5 and 6 the graphs corresponding to the three vibration directions, together with the minimum workmanship for each filter. For the WR75 filter, as shown in Figure 5 the presence of resonances above 1000 Hz can be observed in the tests carried out on the X and Z axes. This is due to the resonance produced by the aluminum supports that hold the device, which could be eliminated by reducing the length of these supports. For the C-SMT and R-SMT filters, as shown in Figure 6 the vibrations excited on the test bench (measured) are practically always above the minimum workmanship. There are only two areas where the minimum workmanship has not been exceeded: below 20 Hz the desired power level cannot be achieved in order to safeguard the integrity of the mechanical exciter, and above 1200 Hz the test bench presents resonances that modify the spectrum.

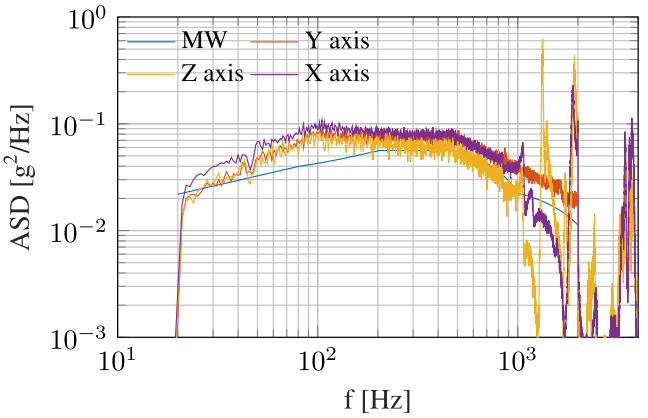

FIGURE 5. Amplitude Spectral Density (ASD) of vibration applied to WR75 filter in random vibration tests.

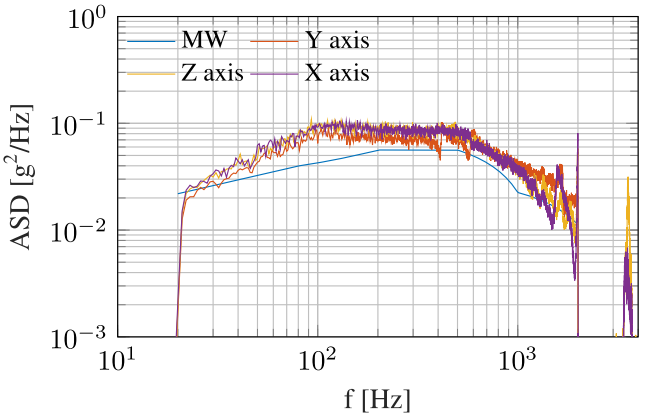

FIGURE 6. Amplitude Spectral Density (ASD) of vibration applied to C-SMT and R-SMT filters in random vibration tests.

D. NATURAL FREQUENCY

Mechanical systems have natural frequencies of resonance. When a system is excited with a mechanical field that oscillates at the natural frequency, the system enters into resonance, and the amplitude of the vibrations increases substantially. Therefore, the measurement of this parameter is critical because it is representative of the structural integrity of a system.

Usually, during a vibration test campaign, the devices' natural frequency is measured before and after each test is performed. According to the standard, the deviation in natural frequency after each test must be under 5%, and the variation in amplitude under 20%. Not fitting these constraints is a symptom of the loss of mechanical integrity of the system or device.

In this work, the natural frequency was measured before and after having completed the two performed tests (sinusoidal sweep and random vibration). Therefore, the natural frequency variation was due not to one but two tests, thus adding an inherent safety margin to the ECSS standard.

To carry out the measurement, an ultralight accelerometer (weight: 0.5 g) was installed on the central section of each filter by using a non-permanent adhesive, see Figure 3. In this way, we obtain the transfer function between the acceleration measured at that point and the acceleration applied to the base, so that the natural frequency and its amplitude can be easily extracted. As excitation, it was used a random signal with a frequency content of up to 2000 Hz and an amplitude lower than RMS 0.8 g. This test is carried out with the modules located in position Y (upper photographs of Figure 3).

E. RESULTS

The electric frequency response of every filter was measured by using a Vectorial Network Analyzer (VNA), before and after the vibration tests, at ambient temperature (25 °C). Two TRL calibration kits (one in WR75 waveguide and the other one in microstrip) were used to eliminate the effect of connectors and feeding lines. Figures 7, 8 and 9 presents the resulting measurements.

The results show that the changes in the frequency response are negligible in terms of the return or insertion loss in the passband, or in terms of the frequency shifts, and they can be blamed on a repetition of the measurement rather than on the effect of the vibration tests.

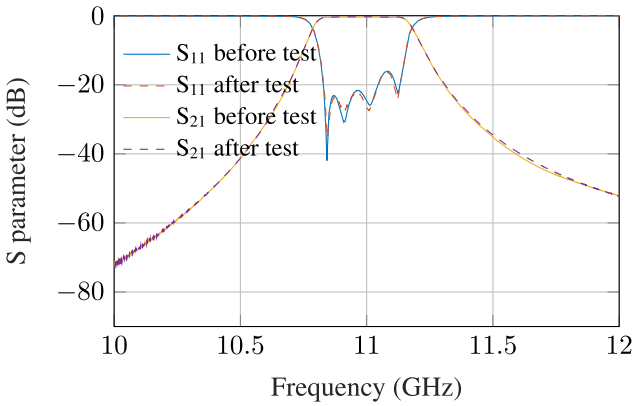

FIGURE 7. Frequency response of the WR75 filter before and after vibration tests.

On the other hand, Table 1 shows a comparison between the natural frequencies and amplitudes for the three filters before and after performing the tests. As previously mentioned, the ECSS standard established a maximum variation of 5% in the natural frequency, and 20% in amplitude for the viability of the device under test (DUT). None of the filters has experienced variations greater than the established limits. In the case of the C-SMT filter, a slight increase in the natural frequency obtained after the test is observed. This may be caused by an increase in the tightening torque of the fixing screws to the platform (this module had to be disassembled to change the test configuration from horizontal to vertical).

IV. THERMAL STABILITY TESTS

Communications satellites are exposed to periods of sun and shade throughout their life cycle. When the satellite is in a sunny period, the solar radiation falls squarely on it, causing

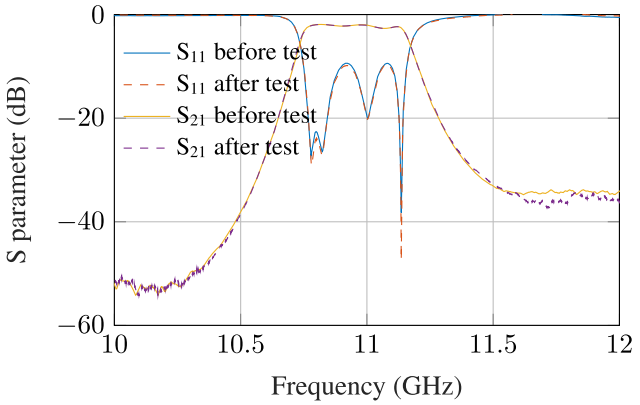

FIGURE 8. Frequency response of the R-SMT before and after vibration tests.

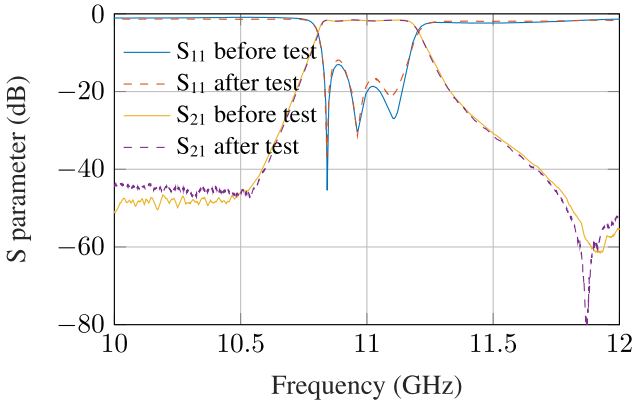

FIGURE 9. Frequency response of the C-SMT filter before and after vibration tests.

TABLE 1. Variation of the natural frequencies of the filters after carrying out the set of vibration tests.

Filter	Nat. Frec. (Hz)	Δf (%)	Amplitude	ΔAmp. (%)
R-SMT	433-432	-0.2	223.4-235.6	5.5
C-SMT	615-621	1.0	198.2-170.0	-14.2
WR75	1772-1768	-0.2	220.5-202.5	-8.2

its temperature to increase. Similarly, when the satellite is in a period of shadow, it radiates heat, thus reducing its temperature. These temperature changes depend on the orbit of the satellite and are unavoidable, so the payload must guarantee its operation within the wide range of temperatures expected during its operation.

Temperature tests are required to validate the good performance of microwave devices for space applications. These tests evaluate the variation of the frequency response of space payload devices within a wide temperature range. References [18], [19], and [20] study the temperature gradients that are experienced by low orbit satellites, as well as their electronic systems and antennas. As a conclusion, a range of temperatures from -20 to 40 °C is required for filters on board of LEO satellites. Nevertheless, higher orbit satellites would require a wider range of temperatures. To be compliant with the requirements of ECSS for thermal tests of LEO and higher orbit satellites, a range of temperatures from −60 to 90 °C was employed, including measurements at −60, −40, −20, 0, 20, 40, 60 (maximum temperature for antennas in LEO satellite) and 90 °C (maximum operating temperature of the metalization).

This analysis has been used to define the tests to measure the electrical response versus temperature of the WR75 filter and the C-SMT filter. The measurement has been carried out in the High Power Radiofrequency Space Laboratory of the European Space Agency (ESA) and the Valencian Space Consortium (VSC), whose specifications and configuration can be found in Section IV-A, and whose results are included in Section IV-B.

A. SET-UP FOR THERMAL STABILITY TESTS

These tests have been performed following the technical specifications for testing the different systems and devices used for space engineering [12]. In particular, those required for the standardization of payload equipment, generally including waveguides and waveguide based devices, as it is the case of the considered filters. The tests were performed under atmospheric pressure conditions, since the work developed in [10] shows that there was no substantial difference in thermal response for tests performed under atmospheric or high vacuum conditions.

The measurement setup consists of a temperature chamber (Vötsch VT70010) and a vector network analyzer (VNA). Inside the thermal chamber, there are several temperature sensors. Some of them are placed on a chamber wall, and the others on the DUT.

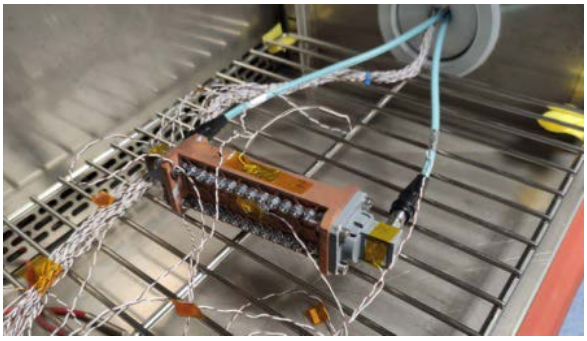

FIGURE 10. WR75 filter inside the climatic chamber.

The measurements consisted on introducing the devices, one by one, inside the thermal chamber while they are connected to a VNA (see Figure 10). The thermal chamber adapted the device temperature to the target profile one. Every time the temperature has reached one of the the targets in the profile, the electric response of the device is stored after a dwell time.

Two TRL calibration kits were developed (one for the WR-75 filter and the other one for the C-SMT filter). Nevertheless, the VNA was not calibrated before measuring the filters, since that would assume that the responses of the

TRL calkit standards (Thu, Reflect and Line) did not change with temperature. On the contrary, the electric responses of calkit elements were measured at each one of the target temperatures. Thereafter, these measurements are used to calibrate the responses of the two filters by using a Matlab function, that allows to obtain the corrected measurement at each one of the temperatures following the procedure described in [21].

For the C-SMT filter, welded SMA connectors with a working temperature range from -65 °C to 165 °C were used.

B. RESULTS OF THERMAL STABILITY ANALYSIS

Figures 11 and 12 depict the transmission coefficients of the filters after applying the external TRL temperature calibration procedure at each temperature, under atmospheric pressure.

For both filters, the test performed 3 measurements at 20 °C: at the start, in the middle and at the end of the cycle. The objective was to observe permanent changes of the electric response due to the temperature testing. For the WR75 filter the maximum shift was 0.033% for center frequency, 1.188% for bandwidth and 0.039 dB for insertion loss. For the C-SMT filter these variations were 0.010% for center frequency, 1.679% for bandwidth and 0.079 dB for insertion loss. In both cases the deviations are so low that do not imply any permanent change in the device.

Analysing the data of Figure 11, it can be stated that the center frequency of the WR75 filter is inversely proportional to the temperature, thus following the expected behavior, since when lowering the temperature the material contracts and smaller cavities imply higher frequencies. This proportion is lineal with a slope of -0.4274 MHz/°C and a maximum deviation of 33.3 MHz (-0.301%). On the other hand, the bandwidth at -3 dB has been more affected because its value depends on all the dimensions of the device and not only on the lengths of the resonators, as it is the case of the central frequency. The variation follows a lineal function with a slope of 0.0572 MHz/° and a maximum value of 14.25 MHz (3.76%). Insertion loss follows an inverse relationship with temperature (-0.0064 dB/°C), since most of this loss are due to the gap between the two parts of the device. In this way, when the temperature increases, the device expands and the gap between both parts is reduced.

Observing Figure 12, the same inverse lineal relationship between center frequency and temperature appears for the C-SMT filter, with a slope of −0.1791 MHz/°C and a maximum deviation of 16.4 MHz (−0.15%). The bandwidth at −3 dB presents a higher variation, as in the case of WR75 filter and for the same reasons. Likely the trend is lineal with a slope of −0.0418 MHz/°C and a maximum value of 10.5 MHz (2.61%). Insertion losses increase with temperature at a rate of 0.0030 dB/°C. However, in this device the largest source of losses is found in the input microstrip line, where we will find losses due to dielectric, conductor and radiation that increase with temperature.

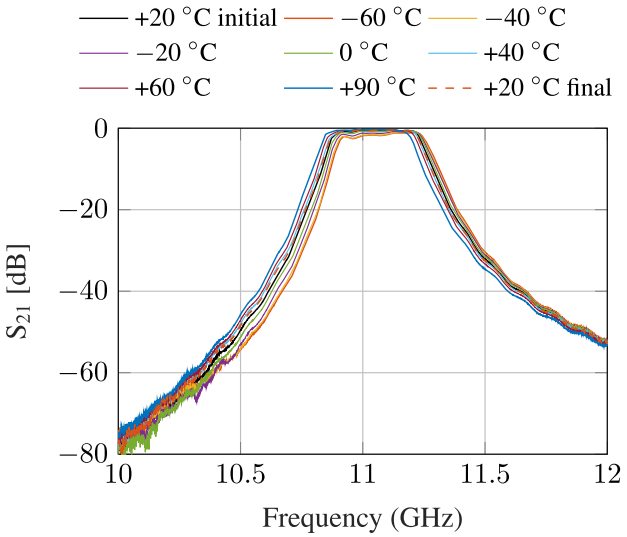

FIGURE 11. WR 75 filter response during the temperature test.

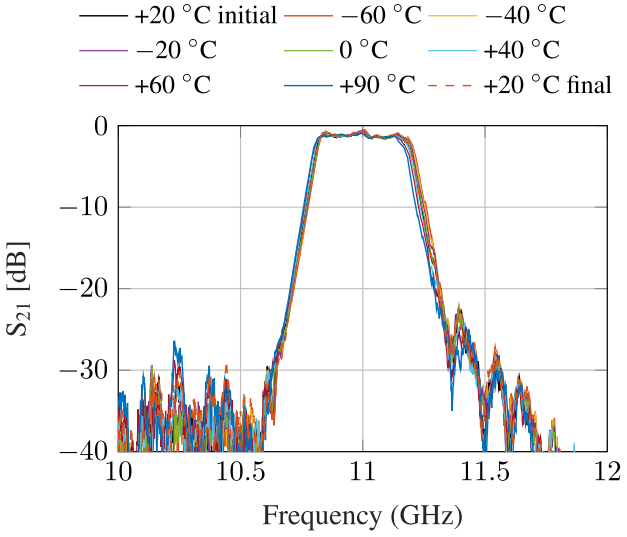

FIGURE 12. C-SMT filter response during the temperature test.

V. POWER HANDLING: MULTIPACTOR PHENOMENON

The multipactor phenomenon is an avalanche discharge of electrons that occurs in communications devices working with high-power electromagnetic (EM) fields under low pressure [22], [23]. When these conditions meet, free electrons inside the device are accelerated by the electric field, eventually impacting the metallic walls of the device. If the intensity of the applied field is high enough, the collision of an electron (primary electron) can release more than one electron from the metal surface (secondary electrons). These secondary emitted electrons can be accelerated towards other metallic walls releasing, in turn, more electrons. If this process is in resonance with the RF field, more secondary electrons will be generated in each cycle, producing an exponential growth of free electrons. This cluster of electrons can result

in several harmful effects such as increment of the electric noise, undesired power reflections, detuning of resonators and filters, as well as heating of the device. Moreover, it is known that a multipactor discharge can also start a corona discharge that can ultimately destroy the device [24]. Since satellites can not be repaired in orbit, prediction and testing of harmful effects such as multipactor or corona discharge are crucial to ensure the correct operation of the satellite throughout its lifetime [25].

Multipactor is a complex phenomenon that strongly depends on several factors that should be measured or approximated before testing: the electrical response of the device, the power and frequency of the RF fields, the electron-free distance, and the Secondary Electron Emission (SEE) properties of the involved surfaces. In this work, a study of the critical frequency and areas of the proposed devices is explained in Section V-C. The secondary electron emission properties of the devices' surface were quantified by measuring the Secondary Emission Yield (SEY). This measurement was carried out at the European Laboratory of High Power Materials for Space of ESA and VSC, and the results of this test can be found in Section V-B. As part of the analysis, the outgassing of the material due to heating was approximated through a ThermoGravimetric Analysis (TGA), the relating results can be found in Section V-A.

As a result of the previous analysis, the devices were manufactured and recursively re-designed until an EM response close enough to the ideal one was achieved. In this way, we can assume that the multipactor discharge study is valid. Finally, the devices were delivered to the European High Power Radiofrequency Space Laboratory of ESA and VSC, where their multipactor discharge threshold values were measured under vacuum conditions, i.e. the minimum RF power that can trigger a multipactor discharge. The test setup meets the requirements of the ECSS-E-20-01C standard [25] and the test description and results are exposed in Section V-D.

A. THERMOGRAVIMETRIC ANALYSIS

The space communications industry is often reluctant to use new materials and technologies unless they are tested in a wide range of scenarios. One of these is the outgassing rate, which is the release of gas that was dissolved, trapped or frozen in the material. This include boiling, sublimation or evaporation of the material itself and desorption and seepage of water and other components of the material under study.

In high vacuum environments, the generation of volatile species can be detrimental, as it can condense in unwanted places or instruments. In the case of space satellites, the gas can condensate in critical instruments such as solar panels or optical systems, ultimately reducing their efficiency. This condensation can also contaminate the pricey instrumental of the testing vacuum chambers during testing campaigns. In addition, the release of gas in microwave devices that work under high power signals, can transform a multipactor discharge into a very harmful corona discharge [26]. In such a discharge, free electrons inside the device collide with the gas molecules extracting secondary electrons from them. This process, sustained over time, ionises the gas and produces extreme heating that can destroy the communication component and derail the space mission. For these reasons, it is advisable to verify that no harmful gases are released during device testing or during regular satellite operation. In fact, the CSS-Q-ST-70-02C standard states that an outgassing analysis should be applied to materials that are exposed to temperatures higher than 125 °C for short periods or to temperatures higher than 50 °C for longer periods (over one week).

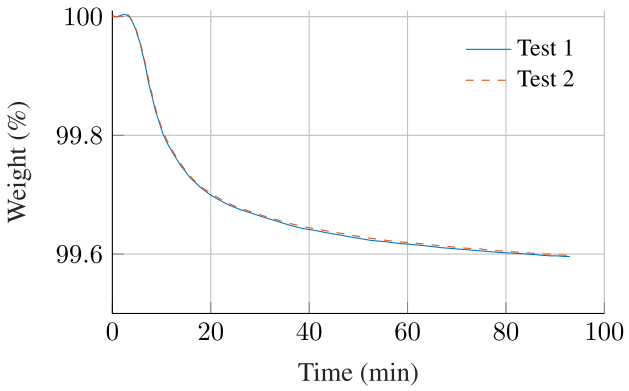

FIGURE 13. ThermoGravimetric Analysis (TGA) results of a Rigid 10K resin sample after thermal curing.

In order to clarify whether the resin used in the proposed manufacturing process is suitable for high vacuum and high power environments, a ThermoGravimetric Analysis (TGA) was carried out in the facilities of the Technological Institute for Children's Products and Leisure (AIJU, by its initials in Spanish). TGA is a technique used to determine the thermal stability of a material by measuring the fraction of volatile components. The purpose of this analysis is to quantify the generation of volatile species of the material when it is heated to a specific temperature and determine, if possible, whether the gas released corresponds to a loss of moisture or to evaporation of the material. In order to do so, a sample of the material is heated at a constant rate or set at a constant temperature while its weight change is monitored. In this case, two samples of Rigid 10K resin of about 83 mg were preconditioned at room temperature (22 ± 1 °C) with a relative humidity of 55 ± 5% for 72 hours to reduce the presence of moisture in the samples. Then, each sample was heated from 30 °C to 125 °C at 20 °C /min in a N_2 atmosphere. Afterwards, the temperature was maintained at 125 °C for 90 min while the weight of the sample was monitored.

Figure 13 shows the results of the two TGA tests. As can be seen, both samples lost a 0.11% of mass the first 10 minutes of the isothermic stage. Then the samples rapidly lost mass during the first minutes at 125 °C, but it stabilised after 90 minutes resulting in a total mass loss of approximately 0.4% (see Figure 13).

After each test, both samples were preconditioned again at at room temperature with a relative humidity of 55 ± 5%.

After this process, both samples gained the mass lost during the ThermoGravimetric test. Based on this, it is highly likely that the mass loss was due to the evaporation of accumulated moisture rather than the evaporation of the resin. Water vapour is not considered a critical containment for vacuum instruments, and although it may start a corona discharge on space instrumentation, this can be prevented by proper drying. Moreover, ESA states in ECSS-Q-ST-70-02C standard [27] that the maximum mass loss allowed for the use of plastic material in vacuum conditions is 1%, which is more than twice the mass loss observed in the tests. Although TGA does not precisely represent the outgassing analysis recommended in the ECSS-Q-ST-70-02C standard, the good results of TGA analysis suggest that Rigid 10k resin can be used in high vacuum environments at temperatures up to 125 °C without significant problems.

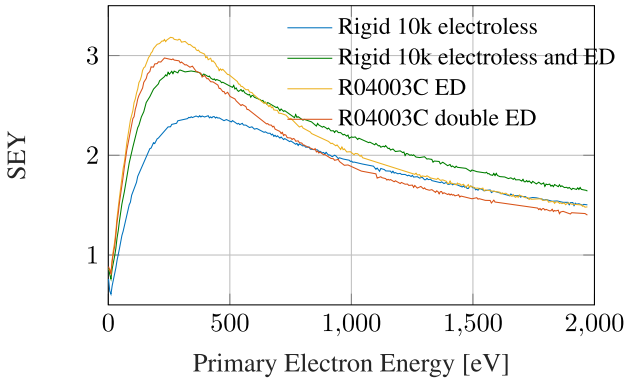

FIGURE 14. Normal incidence SEY curves for different combinations of materials and surface finishing.

B. SECONDARY EMISSION YIELD MEASUREMENT

As was mentioned before, multipactor is strongly related to the secondary electron emission properties of the surfaces where this effect takes place; therefore, the study of multipactor is deeply connected to the study of SEY. This effect exhibits a random nature that depends on many parameters: the energy and angle of impact of the primary electron and the characteristics of the surface (material, roughness, impurities, aging, etc.). As a result, there are no universal SEY curves for each material [28], and measuring the SEY of particular devices, i.e. a combination of material and surface finishing, is essential for an accurate multipactor prediction.

Proposed WR75 devices are generally made of ceramic-filled resin with a double copper coating process. However, SMT devices are made of two different materials, the 3D-printed part and the PCB. Thus, we decided to measure the SEY of 4 different combinations of materials and finishing:

- A sample of RO4003C substrate with a standard electrodeposited (ED) copper cladding of 18 μm.
- A sample of RO4003C substrate with the standard ED coating and an additional ED cladding performed in our facilities.
- A sample of 3D-printed rigid 10k resin with the first electroless cladding.
- A sample of 3D-printed rigid 10k resin with the first electroless cladding and the additional ED cladding performed in our facilities.

Samples were manufactured and metallised with the same processes employed for the final devices to accurately represent the surfaces where multipactor is supposed to appear. Then SEY of each sample, with a normal incident angle, was characterised at room temperature in the European High Power Space Materials Laboratory of VSC-ESA.

Extracted SEY curves present the typical SEY behaviour, see Figure 14. For low energies SEY is below the unity, which means that electrons are absorbed or backscattered. As the energy increases, the SEY increases exceeding the unity, i.e. there is electron multiplication. SEY growth until the maximum (δ_{max}) is reached for a certain energy (W_{max}) when it starts to decrease, and eventually drops below the unity [22]. Extracted δ_{max} in the 3D printed samples is lower than that measured on PCBs, whereas W_{max} is higher for the 3D-printed samples. This seems to be due to the fact that the roughness of 3D-printed surfaces is higher than that of a standard PCB. On the other hand, it can be noticed that the SEY of the samples with the final electroplating carried out in our facilities is higher than the one of the other two samples. In the case of 3-D printed devices, the last finishing is performed to correct minor manufacturing defects and achieve a thicker and more homogeneous plating, so it can be avoided in case that a higher multipactor threshold were needed. However, in the case of PCBs, it is necessary when the layout has Plated Through Holes (PTH) which is very common in most high-frequency circuits.

C. MULTIPACTOR ANALYSIS AND SIMULATION

It was decided to study and test the multipactor discharge threshold of a standard WR75 filter realisation and an SMT low profile filter. As was mentioned before, the surface assembling configuration of the low profile filter is not convenient for multipactor testing as standard coaxial connectors cannot handle the high power needed to start a multipactor discharge. Thus, the structure of the low profile filter was modified to allow its multipactor testing. A WR75 waveguide transition replaced the SMT assembly while the PCB cover was maintained on the filter area, see Figure 1 (d). This new filter realisation features secondary emission properties and electron-free distances comparable to the surface-mounted design, so it has the same multipactor power threshold and electric response as the original SMT filter. The WR75 transition was designed as a three-stage Chebyshev matching transformer [29] obtaining a back-to-back RL of 40 dB in the filter passband. Figure 15 shows the measured response of both filters: the standard WR75 and the low profile realisation. Since multipactor tests are potentially destructive, several prototypes of the WR75 filter were manufactured. The prototype used for the vibration and thermal tests was different

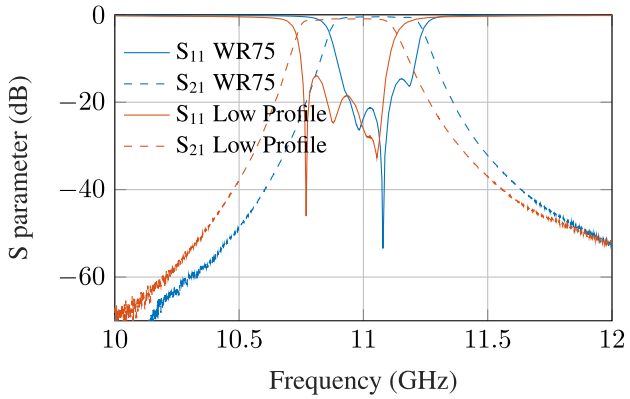

FIGURE 15. Frequency response of the WR75 and Low Profile filter realisations for the multipactor test.

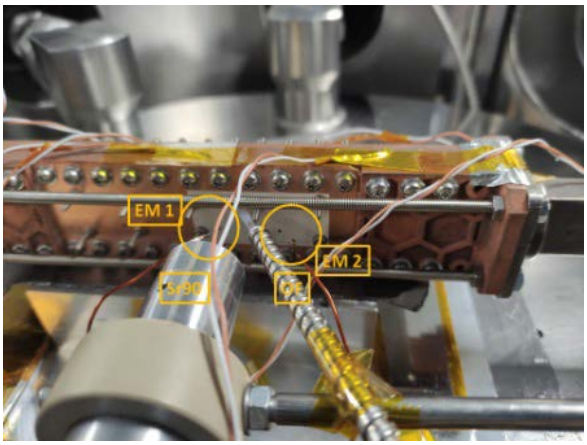

FIGURE 16. Detail of the low profile filter in the multipactor test bench.

than the one used for the multipactor evaluation. Moreover, this allowed us to perform the different tests simultaneously.

It is highly advised to perform a multipactor analysis before testing in order to identify the different factors that impact the multipactor discharge. This analysis includes the following steps:

1) Identify the frequencies and regions where it is most likely to appear a multipactor discharge with the lower RF power level, i.e. critical frequencies and areas.
2) Approximate a worst-case multipactor power threshold using a simple model.
3) Determine an accurate power threshold using a more precise multipactor model.

The first step is to identify critical frequencies and regions of both Devices Under Test (DUTs). In this way, a Time-Average Stored Energy (TASE) analysis can provide the frequency distribution of the electric and magnetic stored energies of the different filter resonators [23], [30]. This analysis allows to identify the frequency and resonator with a higher stored energy and then with a higher electric field. Those regions and frequencies exhibit a higher electron acceleration; thus, the multipactor discharge starts with a lower RF power.

In order to compute the TASE, we firstly extract the actual matrix coupling of both DUTs from their measured responses, Fig, 15. Matrices 1 and 2 depict the extracted coupling matrix of the WR75 and low profile realisation respectively. This was done using the Filter Designer module of CST Studio Suite v.2021, CST GmbH, now with Dassault Systèmes.

$$\begin{pmatrix} 0 & 1.019 & 0 & 0 & 0 & 0 \\ 1.019 & -0.398 & 0.868 & 0 & 0 & 0 \\ 0 & 0.868 & -0.413 & 0.674 & 0 & 0.008 \\ 0 & 0 & 0.674 & -0.382 & 0.863 & -0.141 \\ 0 & 0 & 0 & 0.863 & 0.086 & 1.045 \\ 0 & 0 & 0.008 & -0.141 & 1.045 & 0 \end{pmatrix} \quad (1)$$

$$\begin{pmatrix} 0 & 1.083 & 0 & 0 & 0 & 0 \\ 1.083 & 0.348 & 0.939 & 0 & 0 & -0.001 \\ 0 & 0.939 & 0.452 & 0.730 & 0 & 0.004 \\ 0 & 0 & 0.730 & 0.405 & 0.930 & -0.133 \\ 0 & 0 & 0 & 0.930 & 0.682 & 0.997 \\ 0 & -0.001 & 0.004 & -0.133 & 0.997 & 0 \end{pmatrix} \quad (2)$$

Then the TASE of each resonator can be computed from the low-pass prototype of the filter using the extracted coupling matrix as stated in [23] and [30].

In order to identify the critical frequency, two factors must be considered. On the one hand, the multipactor effect needs lower RF power values at lower frequencies since the product $f \cdot d$ is smaller, which implies a more likely resonance of the electrons with the electric field. However, frequencies with a higher energy concentration will yield higher secondary electron emissions. Thus, attending the TASE of the low-profile filter, see Figure 17, there is no doubt that the critical frequency is located near the lower cut-off frequency, since it is where the lowest frequency in the passband and the concentration of energy is maximum.

On the other hand, the decision is not so simple in the case of the WR75 filter. The upper cut-off frequency presents a greater stored energy than the lower one, see Figure 18. Even presenting a higher $f \cdot d$ product, it is possible that the voltage difference was high enough to produce a multipactor discharge at lower power. Thus, three frequencies should be studied in this case: the lower and higher cut-off frequency and the central one. While only two frequencies will be studied for the low profile filter: the lower cut-off frequency and the central one.

As can be noticed in the TASE (see Figures 17 and 18) the energy is always stored in the second resonator at critical frequencies. This is evident in the standard WR75 realisation. However, the low-profile realisation analysis is more complex since the stored energy is similar in the second and third resonators at the lower cut-off frequency. Hence, this filter realisation requires further analysis and special attention during testing to identify the critical area.

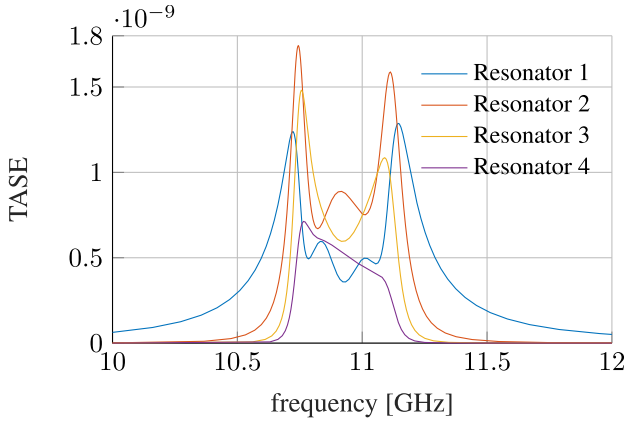

FIGURE 17. TASE of each resonator of the low profile filter.

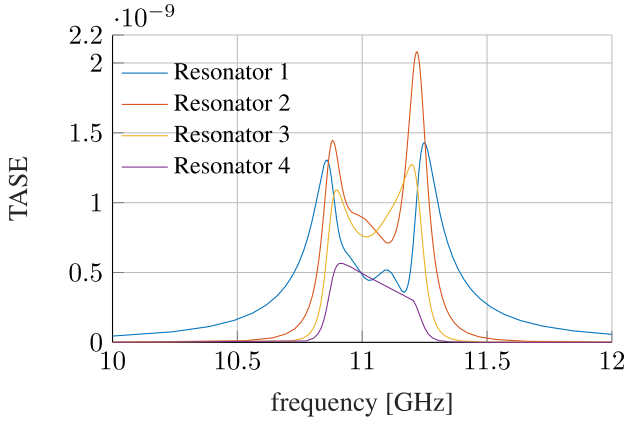

FIGURE 18. TASE of each resonator of the WR75 filter.

On the other hand, communication systems do not transmit at the edge of the passband because the return loss is too high. Communication systems only employ the bandwidth under a certain value of RL. Since the proposed filter realisations do not have tuning elements and present some frequency deviations, we decided to use the bandwidth with a RL higher than 14 dB. Attending to the measured response, the extracted TASE, and practical considerations, it was decided to analyse and test the multipactor phenomenon at the edge of the mentioned practical bandwidth so that the analysis frequencies are 10.917 and 11.199 GHz for the standard WR75 realisation, and 10.775 and 10.940 GHz for the low profile realisation.

Once the analysis frequencies and critical resonators are identified, we simulate the EM fields of both filter realisations at the analysis frequencies. These simulations were used to obtain a first approximation of the power threshold using the well-known parallel plate model of the ECSS multipactor tool [31]. This analysis provides a very conservative threshold, but it can be used to define a starting point in further analyses.

Finally, the previous EM simulations were used to perform several particle simulations on SPAK3D (2021 SP5 - Jun 28 2021). This simulator tracks the trajectory of the initial free electrons (seeding electrons) accelerated by the simulated EM fields, considers the secondary emission effect of the surfaces and analyses the electron population increment. When this increment is high enough, it is considered that a multipactor discharge has occurred. Several simulations have been carried out to obtain the power threshold at the different analysis frequencies. The following simulation parameters were used:

- **Seeding electrons:** 30000 electrons in the case of the low profile realisation, and 50000 in the case of the WR75 filter, both of them universally distributed in the entire device.
- **Multipactor discharge criterion:** by default, the simulator detects a multipactor discharge if the number of electrons increases by an automatically defined factor.
- **Initial power:** 50 W for the low-profile filter and 500 W for the standard WR75 realisation. Both power values are lower than the expected power threshold obtained with the parallel plates model.
- **SEY:** measured SEYs curves of Figure 13 were employed. The explanation of the SEY and the description of the different surfaces of the proposed devices can be found in section V-B.
- **Frequency:** the already defined analysis frequencies and the corresponding centre frequency for each filter realisation have been studied.

The evolution of electron population over time was simulated with different input power levels and for the different analysis frequencies. Figure19 shows the results of this simulation for the low profile filter at the lowest analysis frequency (10.775 GHz). As can be seen, when there is no multipactor discharge, the electrons are absorbed by the material in each impact and the electron population decreases. However, the electron population increases when there is a sustained multipactor discharge. The threshold power is the minimum input RF power at which a multipactor discharge appears, i.e. the minimum input RF power at which the electron population increases exponentially.

Table 2 shows the threshold values of the different devices obtained after the simulations.

D. MULTIPACTOR TEST

Multipactor tests have been performed following the technical specifications for space engineering ECSS-E-ST-20-01C - Multipactor design and test [25]. Tests were performed in the High Power Radio-frequency Laboratory of the ESA-VSC using the test bench depicted in Figure 20.

Pressure was continuously monitored during the different tests, being always lower than 1.5×10^{-5} mbar. Devices were fed by a pulsed continuous wave with an ON time of 20 μs, a 1000 Hz pulse repetition frequency, and a duty cycle of 2%. Test bench was validated and verified with test samples of known breakdown threshold before each test. One Strontium-90 (^{90}Sr) radioactive source was used to simulate the free electrons present in space. The radioactive source was pointed in the direction of the critical area during all multipactor tests.

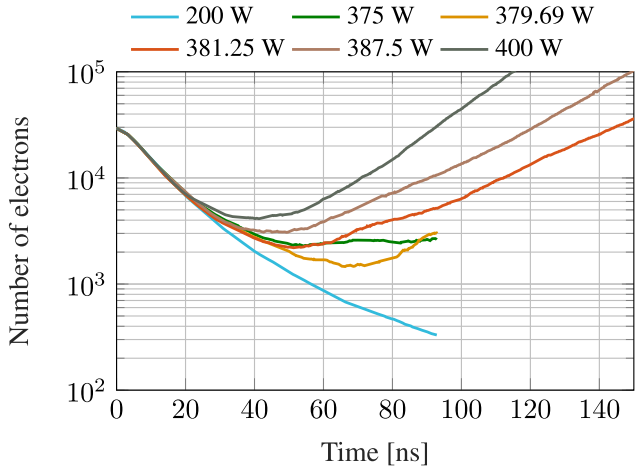

FIGURE 19. Evolution of electron population in a multipactor simulation of the low-profile realisation at 10.775 GHz.

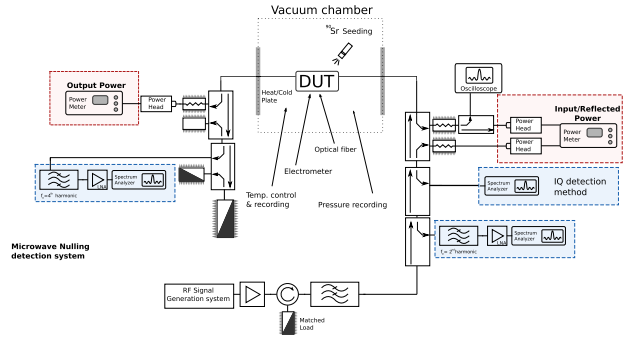

FIGURE 20. Multipactor test setup.

Different multipactor detection methods were employed during the tests: two general detection methods (GDMs) and two different local detection methods (LDMs) to confirm the location of the multipactor discharge.

1) One IQ detection method (GDM).
2) Two harmonic detection methods (GDM).
3) Two electron probe (LDM). One placed in the second resonator and another pointing to the third resonator.
4) One optical detection system (LDM) located in the second resonator.

A multipactor discharge is detected when a change in the response of any detection method is observed. General detection methods are employed to detect the presence of a discharge within the entire device. In fact, these methods detect if a multipactor discharge has occurred in any part of the test bench. Conversely, local detection methods detect the presence of a multipactor discharge in a section of the devices, which helps to discard the presence of a discharge somewhere in the test bed. The ECSS standard criterion [25] establishes that for determining a multipactor power threshold, at least two detection techniques must provide a clear response.

Several holes were performed on both device covers to ease: electron seeding, electron avalanche monitoring, and a correct venting. These sensing and seeding holes were strategically placed to not perturb the EM field neither the multipactor phenomenon but as close as possible to the centre of the resonators, so seeding and electron monitoring could be performed, see Figures 1 (a) and (d).

TABLE 2. Simulated and measured multipactor threshold values.

Filter	WR75			Low-profile	
Frequency (GHz)	10.917	11.051	11.199	10.775	10.940
Simulated multipactor threshold	71 MW	>90 MW	83 MW	380 W	844 W
Measured multipactor threshold	6 kW	No discharge	Not measured	398 W	950 W

Multipactor tests were performed by applying the lowest test power, and then increasing it step by step to the maximum one. When a multipactor discharge is detected, test operators reduce the power until no discharges or events are detected, and increase the power until a new discharge appears. The lower discharge power is then recorded as the discharge threshold. Table 2 shows the measured power thresholds.

The threshold values of the low-profile filter realisation are similar to the estimations obtained with SPARK-3D. The multipactor discharges were detected by the LDM located in the second resonator for both test frequencies, thus confirming that the centre of this resonator is the critical region. In the case of the WR75 realisation, a weak multipactor discharge was observed at 6 kW for the lower analysis frequency. However, this discharge was not detected by any LDM, and it was not confirmed during the verification test. It has to be noticed that the simulated threshold was 71 MW, and since the maximum power of the test bench was 6 kW, it is likely that the detected discharge occurred somewhere in the test bench and not in the device. No additional discharges or multipactor events were observed at other frequencies.

VI. CONCLUSION AND DISCUSSION

This study performed a complete space qualification for several filter realisations with the same electrical response. The filters were developed in different topologies and technologies using additive manufacturing and substrate integration. The complete space qualification implied mechanical stress vibration, thermal stability analysis and power handling with the study of multipactor phenomenon. To the authors' knowledge this is the first time a complete space qualification study is performed on additive manufactured filters made of metallised polymers.

The electric frequency response of the filters (WR75, R-SMT and C-SMT) has been measured before and after random vibration and sinusoidal sweep tests. Both stress profiles are compliant for the main space shuttles: Arianne V and VI, Vega and Soyuz. The results show no significant changes in these responses, no matter the technology used. Furthermore, the deviation of the mechanical natural frequency and

amplitude of the filters was measured. All results are under the 5% and 20% limits respectively.

A complete thermal analysis under atmospheric pressure has been performed for the WR75 and C-SMT filters. The filters have been designed, manufactured and measured at different temperatures according to the ECSS data sheet specifications for thermal testing of devices. The deviations in centre frequency, bandwidth, and insertion loss are small enough to credit the use of both devices in this temperature range. In general, the deviations in centre frequency and bandwidth are comparable with similar studies carried out on substrate integrated filters [10]. Nevertheless, the filters presented in this work have lower variation in insertion loss and a higher return loss, which facilitates their use in the output stage of satellites where high power is needed. The study has extracted coefficients for the deviation with temperature of the most important parameters of the filter, which could help to design mechanisms to compensate temperature effects on the filter response. Furthermore, the devices were measured at room temperature after the test cycle showing no frequency response deviation, proving that the structures did not experience permanent changes due to the thermal stress.

Concerning power handling study, several tests were conducted: thermogravimetric analysis, secondary emission yield and multipactor analysis and measurement. The thermogravimetric analysis showed that the lost mass of the samples under test where due to the evaporation of accumulated water in the material, and the total mass loss is under the 1% limit stated in the standard. After this study, the secondary emission yield of the different surfaces of the materials used for the manufacturing of the filters was characterized. It must be noticed that the materials with a second electrodeposition of copper have higher SEY values, and additive manufactured materials have higher roughness so lower SEY. For the multipactor prediction of the two devices under test (WR75 and low profile filter), the TASE was extracted by using the coupling matrix equivalent prototype, then the critical regions and frequencies (from the multipactor discharge point of view) were identified. Afterwards, a particle simulator was used to determine the power thresholds. Finally, the DUTs were submitted to the multipactor testing in a high vacuum chamber. For the low profile filter the multipactor discharge in the critical frequencies appeared at the same power that was predicted by the simulations. Otherwise, for the WR75 filter the predicted threshold powers in the critical frequencies were so high that the multipactor test bench was not able to reach them, thus confirming the very high predicted values.

The use of polymeric metallised materials for additive manufactured RF devices has successfully passed vibration stress, thermal stability and power handling tests. Therefore, this technology is a good candidate for space applications, specially in the payloads of small satellites at LEO orbits where size, cost, and weight specifications are so critical.

ACKNOWLEDGMENT

The authors want to acknowledge the contribution of Prof. Antonio Besa of Instituto de Ingeniería Mecánica y Biomecánica (UPV). They also wish to acknowledge the help provided by Dr. Carlos Alcaide-Guillén (iTEAM), Mr. Pablo González-Santatecla (iTEAM), and Mr. Óscar Monerris Belda (VSC) for their valuable support in thermal and high power simulations and tests. Finally, they would like to thank the European High Power RF Space Laboratory of the European Space Agency and the Val Space Consortium for contributing with their installations, Laboratory cofunded by the European Regional Development Fund, a way of making Europe.

REFERENCES

[1] A. Zanella, N. Bui, A. Castellani, L. Vangelista, and M. Zorzi, "Internet of Things for smart cities," *IEEE Internet Things J.*, vol. 1, no. 1, pp. 22–32, Feb. 2014.

[2] B. Palacin, N. J. G. Fonseca, M. Romier, R. Contreres, J.-C. Angevain, G. Toso, and C. Mangenot, "Multibeam antennas for very high throughput satellites in Europe: Technologies and trends," in *Proc. 11th Eur. Conf. Antennas Propag. (EUCAP)*, Mar. 2017, pp. 2413–2417.

[3] A. Crisp. (Nov. 2018). *A Price War Coming for SATCOM IoT?*. [Online]. Available: https://www.nsr.com/a-price-war-coming-forsatcom-iot/

[4] SpaceWorks. (Dec. 2020). *Nano/Microsatellite Market Forecast, 10th Edition*. [Online]. Available: https://www.spaceworks.aero/nano-microsatellite-forecast-10th-edition-2020/

[5] L. Qian, S. Li, M. Attallah, T. Skaik, P. Booth, L. Pambaguian, C. M. Espana, P. Martin-Iglesias, and Y. Wang, "Thermal stability analysis of 3D printed resonators using novel materials," in *Proc. 51st Eur. Microw. Conf. (EuMC)*, Apr. 2022, pp. 334–337.

[6] S. Sirci, E. Menargues, and M. Billod, "Space-qualified additive manufacturing and its application to active antenna harmonic filters," in *IEEE MTT-S Int. Microw. Symp. Dig.*, Nov. 2021, pp. 239–242.

[7] A. Reinhardt, M. Mobius-Labinski, C. Asmus, A. Bauereiss, and M. Hoft, "Additive manufacturing of 300 GHz corrugated horn antennas," in *IEEE MTT-S Int. Microw. Symp. Dig.*, Jul. 2019, pp. 40–42.

[8] A. V. G. Subramanyam, D. Sivareddy, V. V. Srinivasan, and V. K. Hariharan, "Realization and qualification of waveguide iris filters for space applications," in *Proc. IEEE Int. Microw. RF Conf. (IMaRC)*, Dec. 2014, pp. 334–337.

[9] T. Martin, "Air-filled substrate integrated waveguide (AFSIW) filters and multiplexers for space application," Ph.D. dissertation, Dept. Electron., Univ. de Bordeaux, France, 2019.

[10] V. Nova, C. B. Martin, J. A. Martinez, H. E. Gonzalez, J. M. Merello, A. B. Martinez, O. Monerris, and V. E. Boria, "Thermal stability analysis of filters in substrate integrated technologies under atmospheric pressure and vacuum conditions," *IEEE Access*, vol. 8, pp. 118072–118082, 2020.

[11] J. M. Merello, C. Bachiller, V. Nova, H. Esteban, and A. Belenguer, "Study of vibration effects on communication filters in substrate integrated technologies," *IEEE Access*, vol. 10, pp. 50418–50426, 2022.

[12] Space Engineering Testing, *ESA Requirements and Standards Division ESTEC*, Standard ECSS-E-ST-10-03C, 2012.

[13] T.-Y. Huang, T.-M. Shen, and R.-B. Wu, "Design and modeling of microstrip line to substrate integrated waveguide transitions," in *Passive Microwave Components and Antennas*, V. Zhurbenko, Ed. Rijeka, Croatia: IntechOpen, 2010, ch. 11, doi: 10.5772/9418.

[14] R. J. Cameron, C. M. Kudsia, and R. R. Mansour, *Microwave Filters for Communication Systems*. Hoboken, NJ, USA: Wiley, Apr. 2018.

[15] *High Resolution SLA and SLS 3D Printers for Professionals*. Accessed: Apr. 4, 2022. [Online]. Available: https://formlabs.com/

[16] Arianespace, Évry-Courcouronnes, France. ARIANE 5 User's Manual. no. 5. Revision 2. Oct. 2016. [Online]. Available: https://www.arianespace.com/wpcontent/uploads/2011/07/Ariane5_Users-Manual_October2016.pdf

[17] Office of the Chief Engineer for System and Subsystem Test, Analysis, Modeling and Evaluation, "Payload vibroacoustic test criteria," Nat. Aeronaut. Space Admin. (NASA), Washington, DC, USA, Tech. Rep. NASA-STD-7001A, Jan. 2011.

[18] P. Preumont, R. Szewczyk, P. Wittels, and F. Czubaczyński, "Heat transfer model of a small size satellite on geostationary orbit," *J. Autom., Mobile Robot. Intell. Syst.*, vol. 13, no. 3, pp. 34–38, Jul. 2019, doi: 10.14313/jamris/3-2019/24.
[19] I. Pérez-Grande, A. Sanz-Andrés, C. Guerra, and G. Alonso, "Analytical study of the thermal behaviour and stability of a small satellite," *Appl. Thermal Eng.*, vol. 29, nos. 11–12, pp. 2567–2573, Aug. 2009. [Online]. Available: https://www.sciencedirect.com/science/article/pii/S1359431108005036
[20] R. Karam, *Satellite Thermal Control for Systems Engineers*. Reston, VA, USA: American Institute of Aeronautics and Astronautics, 1998.
[21] O. M. Belda, E. D. Caballero, J. R. Garnica, and V. E. Boria, "Automatic, calibrated and accurate measurement of S-parameters in climatic chamber," *IEEE Microw. Wireless Compon. Lett.*, vol. 25, no. 6, pp. 412–414, Jun. 2015.
[22] D. González-Iglesias, "Analysis of the multipactor effect in microwave waveguides and transmission lines," Ph.D. thesis, Dept. de Física Aplicada y Electromagnetismo, Universitat de València, May 2017.
[23] P. Gonzalez, C. Alcaide, R. Cervera, M. Rodriguez, O. Monerris, J. Petit, A. Rodriguez, A. Vidal, J. Vague, J. V. Morro, P. Soto, and V. E. Boria, "Multipactor threshold estimation techniques based on circuit models, electromagnetic fields, and particle simulators," *IEEE J. Microw.*, vol. 2, no. 1, pp. 57–77, Jan. 2022.
[24] M. Yu, "Power-handling capability for RF filters," *IEEE Microw. Mag.*, vol. 8, no. 5, pp. 88–97, Oct. 2007.
[25] *Space Engineering—Multipactor Design and Test*, Standard ECSS-E-ST-20-01C, ESA-ESTEC, Noordwijk, The Netherlands, Jun. 2020.
[26] A. D. MacDonald, *Microwave Breakdown in Gases*. New York, NY, USA: Wiley, 1996.
[27] *Space Product Assurance—Thermal Vacuum Outgassing Test for the Screening of Space Materials*, Standard ECSS-Q-ST-70-02C, ESA-ESTEC, Noordwijk, The Netherlands, Nov. 2008.
[28] S. A. Hormigo, "Multipactor in multicarrier systems, theory and prediction," Ph.D. dissertation, Dept. Comunicaciones, Universitat Politècnica de València, Valencia, Spain, Jul. 2014.
[29] D. Pozar, *Microwave Engineering*. Hoboken, NJ, USA: Wiley, 2012.
[30] C. Ernst, V. Postoyalko, and N. G. Khan, "Relationship between group delay and stored energy in microwave filters," *IEEE Trans. Microw. Theory Techn.*, vol. 49, no. 1, pp. 192–196, Jan. 2001.
[31] S. Strijk. (2020). *ECSS MULTIPACTOR TOOL V. 2.0.0*, European Space Agency. [Online]. Available: http://multipactor.esa.int/index.html

CARMEN BACHILLER received the M.Sc. degree in telecommunication engineering and the Ph.D. degree in telecommunication from the Universidad Politécnica de Valencia (UPV), in 1996 and 2010, respectively. From 1997 to 2001, she worked with ETRA I+D Company as a Project Engineer in research and development on automatic traffic control, public transport management, and public information systems using telecommunication technology. In 2001, she joined the Communication Department, UPV, as an Assistant Lecturer, where she has been an Associated Professor, since 2011. She is also teaching electromagnetism theory. She has participated in several research projects, teaching innovation projects, and technological heritage studies. She is the coauthor of 30 research articles and one patent. She is the Curator of the Telecommunications Museum of UPV. Her current research interests include modal methods for electromagnetic analysis, optimization and design of passive microwave structures, analysis and design of substrate integrated transmission lines and circuits, power effects in passive waveguide systems, liquid crystal reconfiguration in microwave passive devices, and 3D manufacturing.

VICENTE NOVA received the M.Sc. degree in telecommunications engineering and the M.Sc. degree in telecommunication technologies, systems and networks from the Universidad Politécnica de Valencia, in 2016 and 2018, respectively. He is currently pursuing the Ph.D. degree with the Institute of Telecommunications and Multimedia Applications (iTEAM), Universitat Politécnica de Valéncia. Since 2018, he has been with iTEAM, Universitat Politécnica de Valéncia. His current research interests include optimization and design of substrate integrated microwave devices, design and manufacture of SICs lines, design and implementation of microwave devices using 3D manufacturing and metalization techniques, and design of reconfigurable devices using anisotropic materials.

ÁLVARO FERRER received the B.Sc. degree in telecommunication technologies and services engineering from the Universidad Politécnica de Valencia (UPV), in 2020. Since 2021, he has been with the Institute of Telecommunications and Multimedia Applications (iTEAM), Universitat Politécnica de Valéncia, where he is currently a Senior Research Technician with the Microwave Applications Group (GAM). His current research interests include design and implementation of microwave devices using 3D manufacturing and metalization techniques.

VICENTE E. BORIA ESBERT (Fellow, IEEE) was born in Valencia, Spain, in May 1970. He received the Ingeniero de Telecomunicación (Hons.) and Doctor Ingeniero de Telecomunicación degrees from the Universitat Politècnica de València, Valencia, in 1993 and 1997, respectively. In 1993, he joined the Departamento de Comunicaciones, Universitat Politècnica de València, where he has been a Full Professor, since 2003. From 1995 to 1996, he held a Spanish trainee position with the European Space Research and Technology Centre, European Space Agency (ESTEC-ESA), Noordwijk, The Netherlands, where he was involved in the area of EM analysis and design of passive waveguide devices. He has authored or coauthored ten chapters in technical textbooks, 180 articles in refereed international technical journals, and over 200 papers in international conference proceedings. His current research interests include analysis and automated design of passive components, left-handed and periodic structures, and simulation and measurement of power effects in passive waveguide systems. He has been a member of the IEEE Microwave Theory and Techniques Society (IEEE MTT-S) and the IEEE Antennas and Propagation Society (IEEE AP-S), since 1992. He is also a member of the European Microwave Association (EuMA) and the Technical Committees of the IEEE-MTT International Microwave Symposium and the European Microwave Conference. He has been the Chair of the 48th European Microwave Conference held in Madrid, Spain. He was an Associate Editor of IEEE Microwave and Wireless Components Letters, from 2013 to 2018, and *Electronics Letters* (IET), from 2015 to 2018. He also serves as a Subject Editor (Microwaves) for *Electronics Letters* (IET) and an Editorial Board Member for *International Journal of RF and Microwave Computer-Aided Engineering*. He acts as a regular reviewer of the most relevant IEEE and IET technical journals in his areas of interest.